Hindawi
International Journal of Polymer Science
Volume 2017, Article ID 9316761, 9 pages
https://doi.org/10.1155/2017/9316761

Research Article

Effect of Graphite Nanosheets on Properties of Poly(3-hydroxybutyrate-*co*-3-hydroxyvalerate)

Larissa Stieven Montagna,[1] Thaís Larissa do Amaral Montanheiro,[1] João Paulo Barros Machado,[2] Fábio Roberto Passador,[1] Ana Paula Lemes,[1] and Mirabel Cerqueira Rezende[1]

[1] *Institute of Science and Technology, Federal University of São Paulo (UNIFESP), Group of Polymers and Macromolecules, São José dos Campos, SP, Brazil*
[2] *National Institute for Space Research (INPE), Associated Laboratory of Sensors and Materials (LAS), São José dos Campos, SP, Brazil*

Correspondence should be addressed to Larissa Stieven Montagna; larissambiental@yahoo.com.br

Received 24 January 2017; Revised 27 March 2017; Accepted 5 April 2017; Published 3 May 2017

Academic Editor: Marta Fernández-García

The influence of different contents, 0.25, 0.50, and 1.00 wt%, of graphite nanosheets (GNS) on the properties of poly(3-hydroxybutyrate-*co*-3-hydroxyvalerate) (PHBV) nanocomposites obtained by solution casting method has been studied. GNS were prepared by three steps: intercalation (chemical exfoliation), expansion (thermal treatment), and the GNS obtainment (physical treatment by ultrasonic exfoliation). X-ray diffraction (XRD), Raman spectroscopy, and field emission gun-scanning electron microscopy (FE-SEM) showed that the physical, chemical, and thermal treatments preserved the graphite sheets structure. XRD and Raman results also showed that GNS were dispersed in the PHBV matrix. The degree of crystallinity (X*c*) of the nanocomposites did not change when the graphite nanosheets were added. However, the GNS acted as nucleation agent for crystallization; that is, in the second heating the samples containing GNS showed two melting peaks. The addition the GNS did not change the thermal stability of the PHBV.

1. Introduction

Problems caused by the environmental pollution generated by polymeric solid waste and petroleum derivatives have led the society to reflect on the development of new materials from renewable sources, for example, the use of natural polymers, in order to minimize the generation of polymeric residues in the environment and pollution caused by its disposal. The development of biodegradable nanocomposite polymeric material with durability and equivalent properties to those presented by thermoplastic nonrenewable sources is very interesting and may replace the nonrenewable composites in the future [1, 2].

Polymer nanocomposites combine one or more components, in which one is a polymer matrix and the other are particles having dimensions that measure up to billionth of a meter (1 nm = 10^{-9} m), in nanometric dimensions. These particles are employed in very low amount (up to 5 wt%) to improve the properties, and the resulting nanocomposites present an extending of applications in engineering, physics, chemistry, and biology [3].

Poly(3-hydroxybutyrate-*co*-3-hydroxyvalerate) (PHBV) is a polyester from the polyhydroxyalkanoates (PHA) family with high degree of crystallinity (X*c*) (55 to 75%) and a low hydrophilic character [4, 5] (Figure 1). PHBV is also a copolymer of polyhydroxybutyrate (PHB) that is isotactic semicrystalline polyester and it is the most well-known polymer of the PHA family [6]. They are naturally occurring biodegradable polyesters produced by microorganism, especially bacteria, which are exposed to carbon source while all other necessary nutrients become limited [7, 8]. The presence of 3-hydroxyvalerate unit (3HV) in the PHBV allows improving the toughness and increases the processability-temperature window [9, 10]. Furthermore, with the

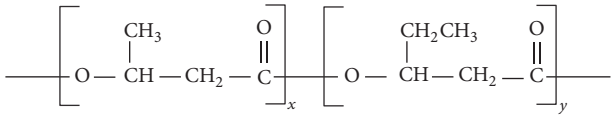

Figure 1: Structural formula of the copolymer poly(3-hydroxybutyrate-*co*-3-hydroxyvalerate).

amount increasing of the HV, the impact strength increases, while melting temperature, degree of crystallinity, and tensile strength decrease in this copolymer.

The graphite nanosheets (GNS) are low-cost fillers, which are obtained through chemical and physical treatments of natural graphite. The GNS are formed by several graphite sheets of a few nanometer thick and from hundreds to thousands nanometer longs connected by van der Waals forces [11]. Furthermore, the graphite nanosheets present conductive, mechanical, and thermal properties; that is, when they are added in a polymer matrix they can improve these properties [12–15].

The number of publications of graphite-based nanocomposites has grown exponentially in recent years, although the number of research papers involving nanocomposites containing graphite and biodegradable polymers is still limited [16, 17]. The interfacial interaction between the polymer matrix and the graphite nanosheets has a key role in the mechanical, thermal, and physical integrity of the corresponding nanocomposites and their final performance.

The molecular interactions of the nanoparticles with polymers are limited to weak van der Waals forces that are universal attractive interactions between molecules generated by the transient or permanent dipoles of the molecules [13, 18]. The improvement of the ultimate properties of the nanocomposites depends on the choice of the most appropriate method for the dispersion of the nanoparticles in polymer matrix (Figure 2) [13, 19, 20]. By solution processing it is possible to obtain dispersed and organized sheets of graphite within polymer matrix, to enhance the nanocomposite performance.

This work aims to develop PHBV nanocomposites reinforced with different contents of graphite nanosheets (GNS) using a solution mixing method in order to compare and to evaluate the thermal and chemical properties, aiming application in durable products for use in the electronic industry, which requires materials with similar characteristics to those of conventional thermoplastics from petroleum derivatives, however, that are biodegradable at the end of their useful life.

2. Experimental

2.1. Materials. PHBV with 4% of 3-hydroxyvalerate (HV) units and Mw of 187,000 g·mol^{-1} was kindly supplied by PHB Industrial, Brazil. The graphite used for the preparation of graphite nanosheets (GNS) was natural graphite flakes (NGF) from Sigma Aldrich (332461). Concentrated sulfuric and nitric acids and ethanol from Chemical Company of Brazil (Vetec) were used as chemical intercalant and oxidizer

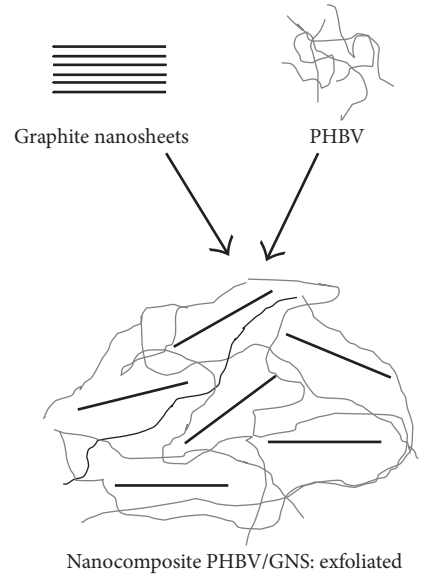

Figure 2: Exfoliated nanocomposite PHBV/GNS.

to prepare the expanded graphite. The solvent used for the film preparation was chloroform ($CHCl_3$), from Synth.

2.2. Method for Obtaining Graphite Nanosheets. The methodology of obtaining the graphite nanosheets was already described by Montagna et al. [21]. The process for preparing the graphite nanosheets is carried out in three steps: intercalation (chemical exfoliation), expansion (thermal treatment), and the graphite nanosheets obtainment (physical treatment by ultrasonic exfoliation). First the natural flake graphite was intercalary with a mixture of concentrated sulfuric acid (H_2SO_4) and nitric acid (HNO_3) (4 : 1, v/v) for 24 h, under appropriated stirring conditions. After that it was washed with distilled water until neutralization and then dried in a furnace above 110°C for 3 h, to remove the remaining water by evaporation, resulting in the intercalated graphite. The dried particles of intercalated graphite were treated at 1000°C for 30 s, thereby obtaining expanded graphite. The graphite nanosheets were obtained by sonication in a 70% of ethanol solution bath for 9 h, after being filtered and dried in a furnace above 100°C for 3 h.

2.3. Preparation of PHBV and PHBV/GNS Nanocomposites Films. The PHBV/GNS nanocomposite was prepared according to the methodology described by Montanheiro et al. [22] and Wang et al. [16]. Initially, graphite nanosheets and chloroform (Synth) (1 : 10 wt/v) were sonicated for 4 h in an ultrasonic bath (Unique, USC1450). PHBV was dissolved in chloroform (1.1 : 10 wt/v) at 40°C. The system remained under stirring until the entire polymer mass has been dissolved and resulted in a viscous solution. Subsequently, the solution containing the graphite nanosheets was stirred with PHBV solution for 3 h at 60°C. The final solution was cast into Petri dishes covered with aluminum foil to obtain films. Afterwards, the solvent evaporated at room temperature for 12 h.

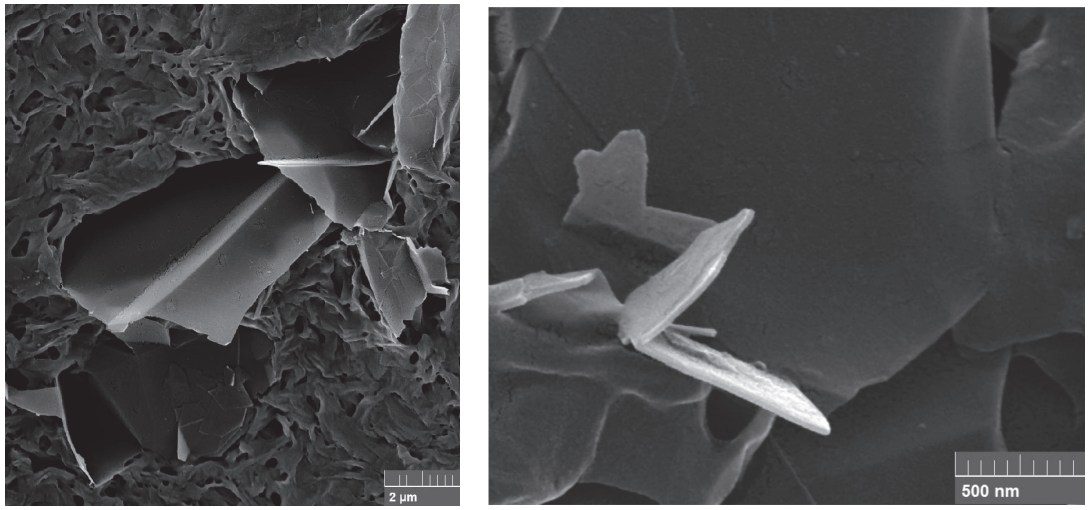

(a) (b)

Figure 3: FE-SEM micrographs of graphite nanosheets with magnification of 20000x (a) and 100000x (b).

2.4. Analytical Characterization

2.4.1. Field Emission Gun-Scanning Electron Microscopy (FE-SEM). Field emission gun-scanning electron microscopy analyses were performed with a TESCAN (model MIRA 3) operating at 5 kV, using aluminum stubs. The samples were sputtered with gold.

2.4.2. Raman Spectroscopy. Raman spectra were carried out using a RamanLabRAM HD Evolution Raman spectrometer (HORIBA), with the laser wavelength of 633 nm as excitation source.

2.4.3. X-Ray Diffraction (XRD). XRD technique was used to determine both the interlayer spacing between stacked graphite nanosheets and the dispersion within the PHBV matrix. Measurements were made in a Panalytical (X'pert Powder) X-ray diffractometer equipped with X'celerator detector. The nanocomposites, in the film form, and the graphite (flakes and nanosheets), in the powder form, were scanned at room temperature, in reflection mode, using incident Cu Kα radiation (k = 1.54 Å) and operating at 45 kV and 40 mA. The data were collected over range of scattering angles (2θ) of 5–50°, time per step of 10 s and step size of 0.02°.

2.4.4. Differential Scanning Calorimetry (DSC). Differential scanning calorimetry analyses were performed on a TA Instruments Q20. Small amounts (5 mg) of dried samples were placed into aluminum pans and subjected to the first heating step from −20°C to 200°C at 10°C min^{-1}, with a isothermal at 200°C for 5 min followed by cooling step to 30°C at 10°C min^{-1}, and the second heating step to 200°C at 10°C min^{-1}, in nitrogen atmosphere with a gas flow of 40 mL·min^{-1}. The degree of crystallinity (Xc) for each sample was determined by

$$\mathrm{X}c\,(\%) = \frac{\Delta H}{\Delta H^{\circ}} \times 100, \quad (1)$$

where ΔH (J·g^{-1}) is the melting enthalpy of the sample calculated from the endothermic peak obtained from the second heating and ΔH° is the theoretical melting enthalpy of the polymer assumed to be 100% crystalline; for the PHBV the value is 109 J·g^{-1} [23].

2.4.5. Thermogravimetric Analysis (TGA). The thermal stability was studied by TGA using equipment from TA Instrument (SDT Q600) at a heating rate of 20°C·min^{-1} from room temperature up to 400°C, under nitrogen atmosphere flow.

3. Results and Discussion

Figure 3 shows the micrographs of graphite in nanometer dimensions obtained after chemical, thermal, and physical treatments. It can be observed that the weak van der Waals forces were broken by ultrasonic vibrational energy, separating the layers in order to obtain sheets with nanometric thickness. Through the micrographs, it was observed that the treatments did not damage the structure of graphene sheets but supported the separation of them.

Raman spectra of nearly all carbon based material exhibit three characteristic bands, denominated as D, G, and 2D [11, 24, 25]. The D peak position, at 1354 cm^{-1}, as a function of excitation energy and for defects in the structure of the graphite, does not correspond to the number of graphene layers; that is, it could be on the amount of disorder present or connected with the rather small size of its particles [26]. The G band is located at about 1576 cm^{-1} and corresponds to the stretching vibration mode. The 2D band at about

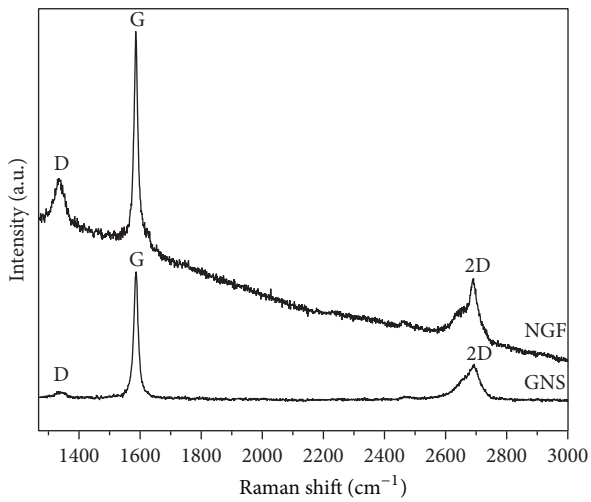

Figure 4: Raman spectra of natural graphite flakes (NGF) and graphite nanosheets (GNS).

2724 cm^{-1} does not require defects for activation, different from the D band. This band is also present in the spectrum of the graphite; the obviously unsymmetrical form of the band evidences the multilayer structure of the original graphite particles [27, 28].

Raman spectra of natural graphite flakes and graphite nanosheets are shown in Figure 4. It was possible to observe the symmetric structure of NGF and GNS. The main characteristic bands of NGF are observed at 2689 cm^{-1} (2D band), 1586 cm^{-1} (G band), and 1333 cm^{-1} (D band). The presence of the D band, with greater intensity, associated with the disorder of the sp^2 carbon, shows the reduction of sp^2 plane size by defects in the structure, vacancies, and distortions of the sp^2 domains and oxygenation of the graphite, that is, defects associated, which are activated by the presence of disorder in carbon systems [29].

In case of graphite nanosheets, the spectrum presents the 2D, G, and D bands at the same wavenumber of the NGF, but with lower intensity, which can be related to the recovery of hexagonal network of carbon atoms with defects, which can be connected to particles with small sizes; that is, the graphene sheets are stacked in an orderly manner [30].

Raman spectra of neat PHBV and PHBV nanocomposites are shown in Figure 5, which has been utilized to evaluate the influence of different contents of GNS and the dispersion of these nanoparticles in the PHBV matrix and their mutual interaction. The spectrum of neat PHBV presents characteristic bands in the range of 2800 to 3100 cm^{-1}, which were assigned to C-H from methyl, methylene, and methyne groups (Figure 5(c)). The strong bands at 2928 cm^{-1} and at 2969–2999 cm^{-1} are assigned to CH_2 and CH_3 of PHBV, respectively. The band at 1725 cm^{-1} is assigned to crystalline phase while the band at 1740 cm^{-1} is related to the amorphous phase [31, 32]. The spectra of PHBV nanocomposites present the same characteristic bands of neat PHBV, however exhibiting a deformation in the G band that is assigned to the vibration of the C-C bond, at 1577 cm^{-1}, 1580 cm^{-1}, and 1583 cm^{-1} for PHBV/0.25% GNS, PHBV/0.50 wt% GNS, and PHBV/1.00 wt% GNS, respectively. Although this more pronounced intensity was observed for samples containing the lowest (0.25 wt%) and the highest (1.00 wt%) GNS contents in PHBV matrix (Figure 5(b)). This fact can be associated with defects in the structure of these nanocomposites, as the decrease in the intensity of the bands characteristics of GNS (Figure 4) corresponds to better dispersion of the nanosheets in the polymeric matrix [33, 34].

Through the ratio between the intensities of the characteristic bands D (I_D) and G (I_G), it was possible to analyze the structure disorder degree, which is related to the formation of more amorphous structure. Samples of NGF and GNS showed I_D/I_G values of 0.43 and 0.04, respectively. The decrease of the I_D/I_G ratio for GNS is an indication of reduced defects in graphite nanosheets. Higher I_D/I_G ratio for NGF is related to sp^3 defects and disorder of the graphite structure, consequently greater intensity of D band. Results can be confirmed in the spectrum of Figure 4, where it is possible to observe the decrease in the intensity of D band, showing the reduction of defects in the GNS spectrum in relation to NGF, which presents a higher intensity of the D band [25].

Figure 6 shows the XRD diffractograms of the natural graphite flakes and graphite nanosheets. The NGF shows a sharp and narrow peak at $2\theta = 26.6^\circ$, which corresponds to the spacing of 3.5 Å (Figure 6(a)). The diffractogram of GNS shows a decrease of the maximum peak intensity, an enlargement, and a shift peak at lower angles, when compared to GNF. This behavior indicates that the chemical, thermal, and physical treatments promoted the exfoliation of the GNF but did not destroy the basic structure of graphite sheets (Figure 6(b)). These effects are indicated by lower crystallinity of GNS compared to NGF. The increase of defects may be caused by distortion of the orientation of graphene sheets and also by the decrease in the number of graphene sheets stacked in each crystal.

XRD measurements offer some support to evaluate the quality of the graphite nanosheets dispersion in PHBV matrix. Figure 7 shows the XRD diffractograms of neat PHBV and PHBV containing different quantities of GNS. The PHBV diffractogram presents three main peaks at 2θ values of 13.6°, 17.1°, and 30.6°, which correspond to (020), (110), and (200) crystal planes, respectively [9]. The strong peak at approximately $2\theta = 26^\circ$ corresponds to GNS's planes and to the typical d-spacing between the carbon layers in graphite, which are also present in the nanocomposites PHBV/GNS.

Neat PHBV and PHBV/GNS nanocomposites show no significant difference in the peak positions with similar diffraction peaks. This characteristic indicates that the crystal structure of PHBV remains unchanged despite the presence of GNS in the PHBV matrix.

Table 1 shows the values of the distances among graphene sheets and the crystal size of GNS in the PHBV matrix. The basal spacing d_{002} was calculated using Bragg's law. The increase of the basal spacing d_{002}, indicated by the shift of the diffraction peak at lower 2θ angles, is relative to the intercalation of polymer chains into graphite nanosheets, while its disappearance is attributed to the presence of

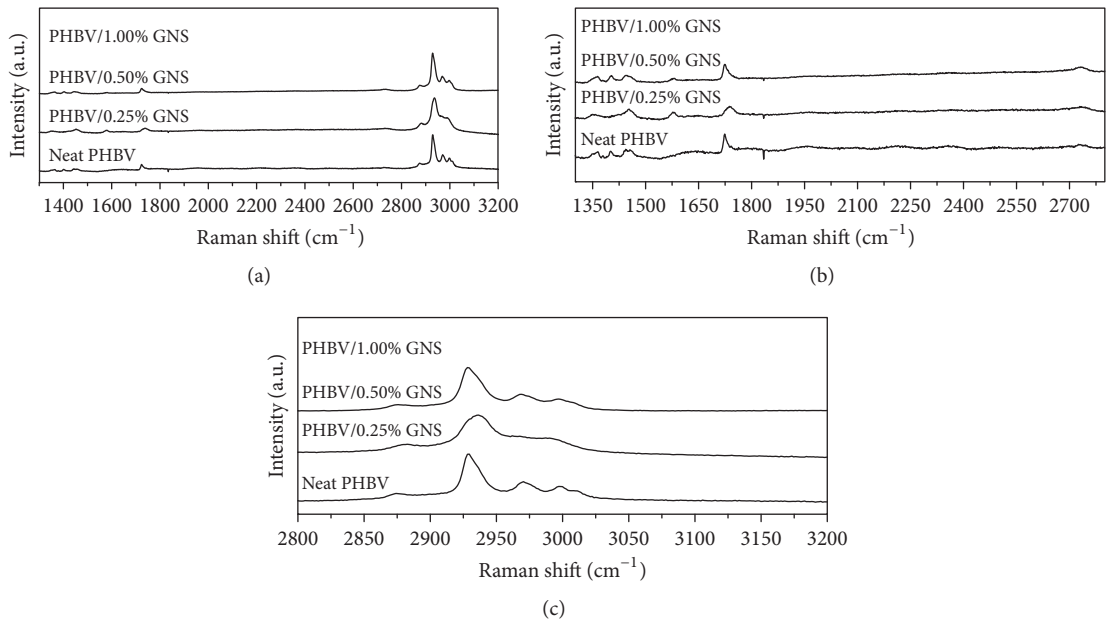

Figure 5: Raman spectra of neat PHBV and PHBV nanocomposites.

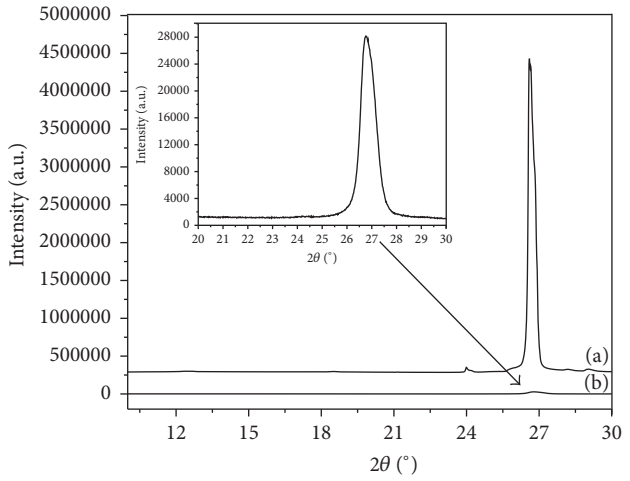

Figure 6: X-ray diffractograms of natural graphite flakes (NGF) (a) and graphite nanosheets (GNS) (b).

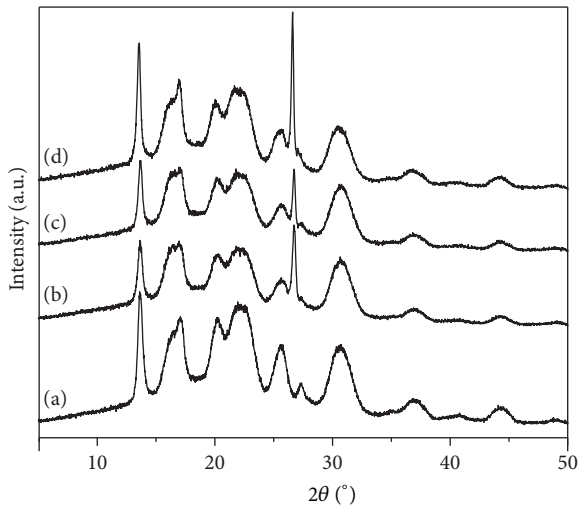

Figure 7: XRD of neat PHBV (a) and PHBV with different concentrations of GNS: PHBV/0.25 wt% GNS (b), PHBV/0.50 wt% GNS (c), and PHBV/1.00 wt% GNS (d).

an exfoliated structure. It was observed that the distance between the layers of graphene, 0.33 nm, was the same in all nanocomposites. The crystal size C (nm) calculated for the reflection peak using Scherrer's equation was 25.6 nm, 35.5 nm, and 35.5 nm in PHBV/0.25% GNS, PHBV/0.50 wt% GNS, and PHBV/1.00 wt% GNS, respectively. These results indicate that the crystallization of PHBV chains is promoted due to the presence of graphite nanosheets.

Thermal analyses were performed on neat PHBV and on the nanocomposites to determine changes in the crystalline phase of the PHBV matrix, particularly in the degree of crystallinity (Xc) and in the melting temperature (T_m). The melting enthalpy (ΔH) obtained from the endothermic peak area is directly proportional to the crystallinity of the material. Table 2 shows the values of the degree of crystallinity of neat PHBV and PHBV/GNS nanocomposites determined

Table 1: Interlayer distances of NGF and the crystal size of GNS in different concentration in the PHBV matrix.

Samples	2θ (°C)	d_{002} (nm)	C (nm)
PHBV/0.25 wt% GNS	26.73	0.33	25.57
PHBV/0.50 wt% GNS	26.73	0.33	35.52
PHBV/1.00 wt% GNS	26.60	0.33	35.50

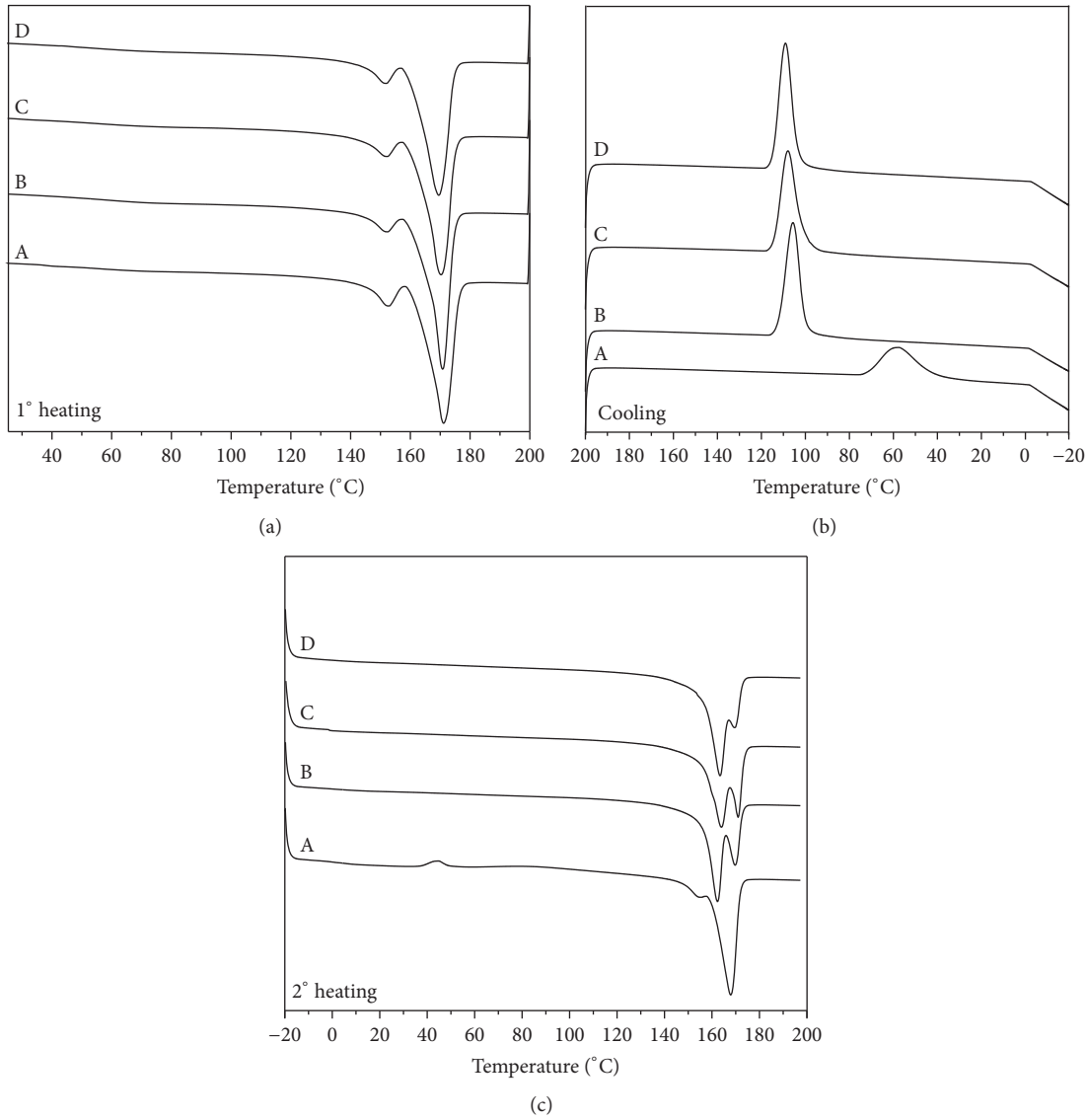

Figure 8: DSC thermograms of the first heating, cooling and second heating runs of neat PHBV (A), PHBV/0.25 wt% GNS (B), PHBV/0.50 wt% GNS (C), and PHBV/1.00 wt% GNS (D).

Table 2: Degree of crystallinity (X*c*) of neat PHBV and PHBV/GNS nanocomposites.

Samples	X*c* (%)
Neat PHBV	73.3
PHBV/0.25 wt% GNS	72.4
PHBV/0.50 wt% GNS	72.2
PHBV/1.00 wt% GNS	71.4

in the second heating scan. It was verified that there were no significant changes in X*c* values with the addition of GNS. Thus, PHBV/GNS nanocomposites present close X*c* values to that determined for neat PHBV. In other words, all the PHBV/GNS nanocomposites are characterized by the same degree of crystallinity, which indicates that the PHBV structure is not impacted by incorporation of graphite nanosheets. This same effect was observed by Crétois et al. [35] that added organoclays into PHBV matrix.

Figure 8 shows the DSC curves for neat PHBV and PHBV/GNS nanocomposites with different contents of GNS (0.25 wt%, 0.50 wt%, and 1.00 wt%). Neat PHBV and the nanocomposites exhibit two characteristic endothermic peaks of melting phenomena. The first peak around 152°C ± 1°C has a weak intensity, while the second peak is obtained at a higher temperature (170°C ± 1°C) and with a higher intensity. On the other hand, a bimodal endothermic melting peak in the first heating scan was observed in all the samples. According to Sridhar et al. [17], this behavior corresponds to the formation of two crystalline phases with different sizes of lamellas of variable thickness, based on hetero and homogeneous nucleation of PHBV.

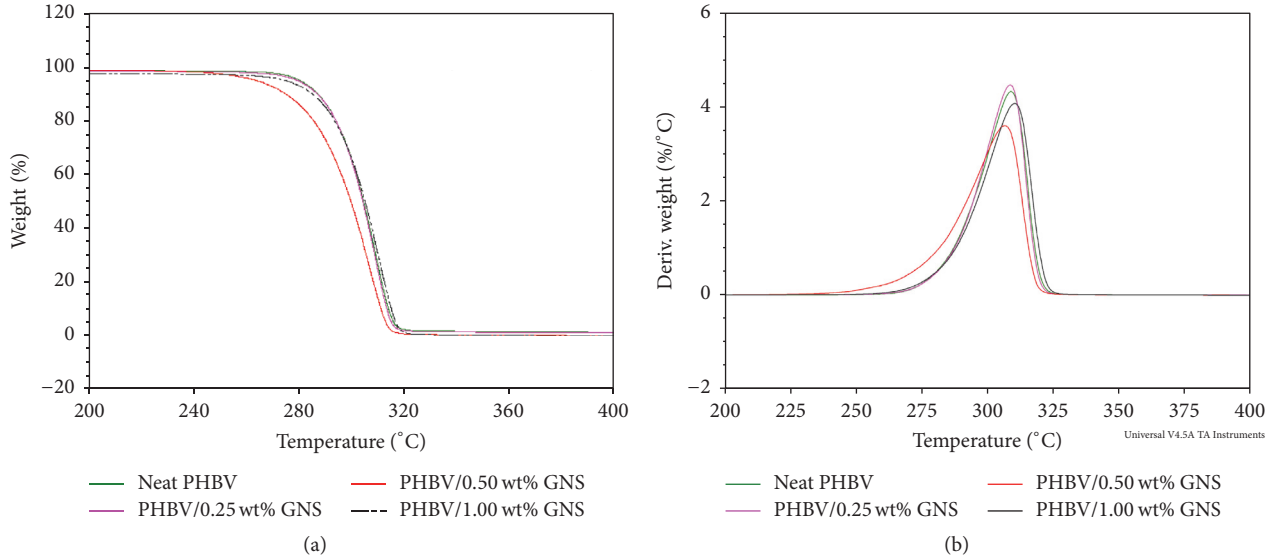

Figure 9: TGA (a) and DTG (b) curves of neat PHBV and PHBV nanocomposites with different GNS contents, 0.25 wt%, 0.50 wt%, and 1.00 wt% of GNS.

After melting, the samples were cooled to −20°C at a rate of 10°C·min^{-1}, and the resulting curves are shown in Figure 8. The sample of neat PHBV showed a small crystallization peak at 58°C during the cooling. However, the PHBV nanocomposites with different contents of GNS showed a large peak of crystallization around 108°C ± 1°C (Figure 8). This fact can be attributed to parts of PHBV that crystallized at the cooling process in the presence of the GNS. This behavior may be related to the presence of GNS that helped in PHBV crystallization in the cooling process, which acted as nucleus for the remaining PHBV to crystallize on the second heating process.

The sample of neat PHBV presented an endothermic melting peak at 168°C, melting temperature slightly lower than that recorded in the first heating. However, the PHBV/GNS nanocomposites showed a double melting peak at two higher nearby temperatures in the second heating, showing a melting-recrystallization-melting process. This can be explained on the basis of hetero and homogeneous nucleation of PHBV, reported in the first melting. This two melting peaks presented at the second heating for the nanocomposites of PHBV/GNS correspond to the heterogeneous nucleation of PHBV with the presence of GNS that occurs due to the chain aggregation and the highest temperature peak is related to the nucleation. This fact indicates that the addition of graphite nanosheets influences both types of nucleation.

TGA analyses were carried out to investigate the effect of the addition of GNS on the thermal stability of PHBV. Figure 9 shows the TGA and DTG curves and Table 3 presents the initial and maximum decomposition temperatures for neat PHBV and PHBV nanocomposites. From the thermogravimetric curves it can be seen that all the PHBV nanocomposites behave similarly to neat PHBV and that the thermal degradation consists of only one weight loss step between 230°C and 310°C (Figure 9).

Table 3: TGA data for neat PHBV and PHBV nanocomposites.

Samples	T_{onset} (°C)	T_{max} (°C)
Neat PHBV	250.92	308.58
PHBV/0.25 wt% GNS	259.02	308.64
PHBV/0.50 wt% GNS	236.52	306.66
PHBV/1.00 wt% GNS	251.74	309.87

T_{onset}: initial decomposition temperature.
T_{max}: maximum decomposition temperature.

This fact indicates no change in the degradation mechanism of PHBV with the incorporation of GNS. However, the addition of GNS to PHBV matrix increases the initial decomposition temperature in approximately 9°C and 1°C for PHBV/0.25 wt% and PHBV/1.00 wt%, respectively. The increase in the thermal stability observed for these nanocomposites may be related to the nanodispersion of the GNS in the PHBV matrix. Although no increase was observed for the sample containing 0.50 wt% GNS, a decrease of 14°C and 2°C in the initial and maximum decomposition temperatures can be observed, respectively (Table 3). According to Sanchez-Garcia et al. [36], a reduction in the thermal degradation temperature was observed with the addition of low amounts of nanoparticles in a PHBV matrix. This behavior was justified by the filler agglomeration, though this behavior was not observed with the addition of lower content (0.25 wt%) of GNS in PHBV matrix. However, in the present study, the sample containing 0.50 wt% of GNS showed a reduction in the thermal stability. This behavior suggests that this sample may have suffered more with the GNS agglomeration in the PHBV matrix, reducing consequently the initial and maximum decomposition temperatures. It is known that the agglomeration of nanosheets in polymer matrix does not contribute with the improvements of nanocomposite properties, such as increased thermal stability.

According to Wang et al. [16], the addition of GNS into the PHBV matrix at low filling content can improve the thermal properties of polymeric matrix. The enhancement of thermal stability is attributed to the high efficiency of GNS for capture free radicals generated by polymer chain scission during the degradation process at high temperatures and due to the homogeneous distribution of GNS in the PHBV matrix.

4. Conclusions

PHBV/GNS nanocomposites with different levels of GNS (0.25 wt%, 0.50 wt%, and 1.00 wt%) were successfully obtained by casting method. Through the diffractograms and the micrographs of the GNS, it was observed that the chemical and physical treatments did not damage the structure of graphite nanosheets. Furthermore, it was possible to observe the decrease in crystal size of GNS in relation to NGF by means of enlargement and shift of the peak at lower angles. XRD and Raman analyses revealed good dispersion of the graphite nanosheets in the PHBV matrix. It was also observed that the crystalline form of PHBV matrix was not affected by addition of GNS, and the nanosheets did not influence the thermal stability of PHBV. The present study provides evidences that the casting method can be successfully applied to develop PHBV/GNS nanocomposites with good dispersion and distribution of the nanosheets into de PHBV matrix.

Conflicts of Interest

The authors declare that there are no conflicts of interest regarding the publication of this research paper.

Acknowledgments

The authors are grateful to CNPq (303287/2013-6 and 158961/2014-5), CAPES/PVNS, and FAPESP (Brazil) for the financial supports.

References

[1] K. Iggui, N. Le Moigne, M. Kaci, S. Cambe, J.-R. Degorce-Dumas, and A. Bergeret, "A biodegradation study of poly(3-hydroxybutyrate-co-3-hydroxyvalerate)/organoclay nanocomposites in various environmental conditions," *Polymer Degradation and Stability*, vol. 119, pp. 77–86, 2015.

[2] L. S. Montagna, A. L. Catto, M. M. C. Forte, and R. M. C. Santana, "Biodegradation of PP films modified with organic prodegradant," *Polyolefins Journal*, vol. 3, p. 59, 2016.

[3] O. Ersen, I. Florea, C. Hirlimann, and C. Pham-Huu, "Exploring nanomaterials with 3D electron microscopy," *Materials Today*, vol. 18, no. 7, article 523, pp. 395–408, 2015.

[4] L. Wing and Y. Jian, "Environmental factors and kinetics of microbial degradation of poly(3-hydroxybutyrate-co-3-hydroxyvalerate) in an aqueous medium," *Journal of Applied Polymer Science*, vol. 87, p. 205, 2003.

[5] G. E. Luckachan and C. K. S. Pillai, "Biodegradable polymers—a review on recent trends and emerging perspectives," *Journal of Polymers and the Environment*, vol. 19, no. 3, pp. 637–676, 2011.

[6] M. M. Reddy, S. Vivekanandhan, M. Misra, S. K. Bhatia, and A. K. Mohanty, "Biobased plastics and bionanocomposites: current status and future opportunities," *Progress in Polymer Science*, vol. 38, no. 10-11, pp. 1653–1689, 2013.

[7] L. N. Carli, T. S. Daitx, R. Guégan, M. Giovanela, J. S. Crespo, and R. S. Mauler, "Biopolymer nanocomposites based on poly(hydroxybutyrate-co-hydroxyvalerate) reinforced by a non-ionic organoclay," *Polymer International*, vol. 64, no. 2, pp. 235–241, 2015.

[8] S. Malmir, B. Montero, M. Rico, L. Barral, and R. Bouza, "Morphology, thermal and barrier properties of biodegradable films of poly (3-hydroxybutyrate-co-3-hydroxyvalerate) containing cellulose nanocrystals," *Composites Part A: Applied Science and Manufacturing*, vol. 93, p. 41, 2017.

[9] J. González-Ausejo, E. Sánchez-Safont, J. Gámez-Pérez, and L. Cabedo, "On the use of tris(nonylphenyl) phosphite as a chain extender in melt-blended poly(hydroxybutyrate-co-hydroxyvalerate)/clay nanocomposites: morphology, thermal stability, and mechanical properties," *Journal Apllied of Polymer Science*, vol. 133, no. 2, Article ID 42390, 2016.

[10] B. Tan and N. L. Thoma, "A review of the water barrier properties of polymer/clay and polymer/graphene nanocomposites," *Journal of Membrane Science*, vol. 514, p. 595, 2016.

[11] K. Krishnamoorthy, G.-S. Kim, and S. J. Kim, "Graphene nanosheets: Ultrasound assisted synthesis and characterization," *Ultrasonics Sonochemistry*, vol. 20, no. 2, pp. 644–649, 2013.

[12] A. P. Kumar, D. Depan, N. Singh Tomer, and R. P. Singh, "Nanoscale particles for polymer degradation and stabilization-Trends and future perspectives," *Progress in Polymer Science*, vol. 34, no. 6, pp. 479–515, 2009.

[13] K. Hu, D. D. Kulkarni, I. Choi, and V. V. Tsukruk, "Graphene-polymer nanocomposites for structural and functional applications," *Progress in Polymer Science*, vol. 39, no. 11, pp. 1934–1972, 2014.

[14] A. Malas, *Progress in Rubber Nanocomposites*, Composites Science and Engineering, Woodhead Publishing, 2017.

[15] J.-C. An, E. J. Lee, and I. Hong, "Preparation of the spheroidized graphite-derived multi-layered graphene via GIC (graphite intercalation compound) method," *Journal of Industrial and Engineering Chemistry*, vol. 47, p. 56, 2017.

[16] B.-J. Wang, Y.-J. Zhang, J.-Q. Zhang et al., "Crystallization behavior, thermal and mechanical properties of PHBV/graphene nanosheet composites," *Chinese Journal of Polymer Science*, vol. 31, no. 4, pp. 670–678, 2013.

[17] V. Sridhar, I. Lee, H. H. Chun, and H. Park, "Graphene reinforced biodegradable poly(3-hydroxybutyrate-co-4-hydroxybutyrate) nano-composites," *Express Polymer Letters*, vol. 7, no. 4, pp. 320–328, 2013.

[18] S. Łoś, L. Duclaux, L. Alvarez, Ł. Hawełek, S. Duber, and W. Kempiński, "Cleavage and size reduction of graphite crystal using ultrasound radiation," *Carbon*, vol. 55, pp. 53–61, 2013.

[19] M. Lai, J. Li, J. Yang, J. Liu, X. Tong, and H. Cheng, "The morphology and thermal properties of multi-walled carbon nanotube and poly (hydroxybutyrate-co-hydroxyvalerate) composite," *Polymer International*, vol. 53, no. 10, pp. 1479–1484, 2004.

[20] H. Wang and Z. Qiu, "Crystallization behaviors of biodegradable poly(l-lactic acid)/graphene oxide nanocomposites from the amorphous state," *Thermochimica Acta*, vol. 526, no. 1-2, pp. 229–236, 2011.

[21] L. S. Montagna, F. D. C. Fim, G. B. Galland, and N. R. D. S. Basso, "Synthesis of poly(propylene)/graphite nanocomposites by in situ polymerization," *Macromolecular Symposia*, vol. 299-300, no. 1, pp. 48–56, 2011.

[22] T. L. D. A. Montanheiro, F. H. Cristóvan, J. P. B. Machado, D. B. Tada, N. Durán, and A. P. Lemes, "Effect of MWCNT functionalization on thermal and electrical properties of PHBV/MWCNT nanocomposites," *Journal of Materials Research*, vol. 30, no. 1, pp. 55–65, 2015.

[23] S. Vidhate, L. Innocentini-Mei, and N. A. D'Souza, "Mechanical and electrical multifunctional poly(3-hydroxybutyrate-co-3-hydroxyvalerate)-multiwall carbon nanotube nanocomposites," *Polymer Engineering and Science*, vol. 52, no. 6, pp. 1367–1374, 2012.

[24] F. Tuinstra and J. L. Koenig, "Raman Spectrum of Graphite," *The Journal of Chemical Physics*, vol. 53, p. 1126, 1970.

[25] N. Soin, S. S. Roy, C. O'Kane, J. A. D. McLaughlin, T. H. Lim, and C. J. D. Hetherington, "Exploring the fundamental effects of deposition time on the microstructure of graphene nanoflakes by Raman scattering and X-ray diffraction," *CrystEngComm*, vol. 13, no. 1, pp. 312–318, 2011.

[26] A. C. Ferrari, "Raman spectroscopy of graphene and graphite: disorder, electron-phonon coupling, doping and nonadiabatic effects," *Solid State Communications*, vol. 143, no. 1-2, pp. 47–57, 2007.

[27] D. S. Lee, C. Riedl, B. Krauss, K. V. Klitzing, U. Starke, and J. H. Smet, "Raman spectra of epitaxial graphene on SiC and of epitaxial graphene transferred to SiO_2," *Nano Letters*, vol. 8, no. 12, pp. 4320–4325, 2008.

[28] O. Y. Posudievsky, O. A. Kozarenko, O. A. Khazieieva, V. G. Koshechko, and V. D. Pokhodenko, "Ultrasound-free preparation of graphene oxide from mechanochemically oxidized graphite," *Journal of Materials Chemistry A*, vol. 1, no. 22, pp. 6658–6663, 2013.

[29] I. S. Elashmawi and L. H. Gaabour, "Raman, morphology and electrical behavior of nanocomposites based on PEO/PVDF with multi-walled carbon nanotubes," *Results in Physics*, vol. 5, pp. 105–110, 2015.

[30] S. S. Maktedar, S. S. Mehetre, M. Singh, and R. K. Kale, "Ultrasound irradiation: a robust approach for direct functionalization of graphene oxide with thermal and antimicrobial aspects," *Ultrasonics Sonochemistry*, vol. 21, no. 4, pp. 1407–1416, 2014.

[31] C. M. S. Izumi and M. L. A. Temperini, "FT-Raman investigation of biodegradable polymers: poly(3-hydroxybutyrate) and poly(3-hydroxybutyrate-co-3-hydroxyvalerate)," *Vibrational Spectroscopy*, vol. 54, p. 127, 2010.

[32] T. Furukawa, H. Sato, R. Murakami et al., "Raman microspectroscopy study of structure, dispersibility, and crystallinity of poly(hydroxybutyrate)/poly(l-lactic acid) blends," *Polymer*, vol. 47, no. 9, pp. 3132–3140, 2006.

[33] S. Yaragalla, A. P. Meera, N. Kalarikkal, and S. Thomas, "Chemistry associated with natural rubber-graphene nanocomposites and its effect on physical and structural properties," *Industrial Crops and Products*, vol. 74, pp. 792–802, 2015.

[34] G. Christopher, M. A. Kulandainathan, and G. Harichandran, "Comparative study of effect of corrosion on mild steel with waterborne polyurethane dispersion containing graphene oxide versus carbon black nanocomposites," *Progress in Organic Coatings*, vol. 89, p. 199, 2015.

[35] R. Crétois, N. Follain, E. Dargent et al., "Microstructure and barrier properties of PHBV/organoclays bionanocomposites," *Journal of Membrane Science*, vol. 467, pp. 56–66, 2014.

[36] M. D. Sanchez-Garcia, J. M. Lagaron, and S. V. Hoa, "Effect of addition of carbon nanofibers and carbon nanotubes on properties of thermoplastic biopolymers," *Composites Science and Technology*, vol. 70, no. 7, pp. 1095–1105, 2010.